The Mechanism of Grain Growth at General Grain Boundaries in $SrTiO_3$

Hadas Sternlicht[1,2], Wolfgang Rheinheimer[3,4], Alexander Mehlmann[1], Avner Rothschild[1], Michael J. Hoffmann[3], and Wayne D. Kaplan[1,*]

[1] Department of Materials Science and Engineering, Technion – Israel Institute of Technology, Haifa 32000, Israel.

[2] Now at the School of Engineering, Brown University, Providence, USA.

[3] Karlsruhe Institute of Technology, Institute of Applied Materials, Karlsruhe, Germany

[4] Now at Technical University of Darmstadt, Germany

* Corresponding author: kaplan@technion.ac.il

Abstract: In this work anisotropic motion of disconnections at general grain boundaries in $SrTiO_3$ was detected in-situ at 1040ºC and 1050ºC using transmission electron microscopy. The same anisotropic motion of ledges and terraces at the surfaces of $SrTiO_3$ was detected in-situ. These results corroborate previous ex-situ studies on disconnection motion in $SrTiO_3$, and experimentally confirm that anisotropic disconnection motion is the mechanism of grain growth.

Key words: Disconnections, grain boundaries, grain growth, surface.

Main Text:

Crystal growth was previously described to occur by step motion, where it was suggested that during growth atoms move along terraces on the surface of a crystal, then along ledges (surface steps) and finally reach kink sites, according to the terrace-ledge-kink (TLK) model, allowing minimization of surface energy [1]. Ex-situ experiments confirmed that ledges and terraces are detectable at surfaces [2-5]. Theoretical models of the atomistic mechanism of grain boundary (GB) migration have been proposed. In one model GBs were characterized according to the TLK model by Gleiter et al., suggesting that GB migration occurs via diffusion of atoms to the GB plane, then atoms diffuse along the GB plane, attach to step sites, and finally diffuse along the step into a kink site [6,7]. This model was partially confirmed by Gleiter using ex-situ transmission electron microscopy (TEM). However, only the projections of the steps were detected, and steps were not directly discerned. In addition, in-situ characterization confirming the motion of steps was lacking. The concept of steps at GBs was extended to line defects which can have both a step and a dislocation character, defined as disconnections by Hirth and Pond, who postulated that disconnections play a key role in the atomistic mechanism of GB migration [8-17]. This model was applied to a number of specific boundaries which were mainly high symmetry coincidence GBs [10-18]. Recently the energy of disconnections was simulated, demonstrating that certain low energy disconnections would be first to form and migrate [19,20].

The projection of steps at general GBs and disconnections at high symmetry GBs were detected using ex-situ [6-23] and in-situ TEM [24-34]. High symmetry GBs are often studied since their atomistic structure can be resolved. However, such model experiments can be far from representative when compared to general high-angle GBs found in polycrystalline systems. To

date, three sets of in-situ experiments confirmed that steps are active during grain growth at specific *high-symmetry* GBs in gold and during shear-coupled migration in aluminum and gold [32-34]. While the observations available in the literature suggest that disconnection motion is the mechanism by which general GBs migrate, this concept requires experimental corroboration. Understanding the mechanism of GB motion is important for both fundamental and applied issues related to microstructural evolution of materials associated with control of the grain size of polycrystalline material systems to optimize their engineering properties.

Recently, general high-angle GBs in $SrTiO_3$ were characterized ex-situ using aberration corrected TEM [35-37]. Anisotropic disconnections were detected along all of the studied boundaries. While the measured GB mobility in $SrTiO_3$ was found to change significantly in a specific temperature range [38-40], both the step and the dislocation components of the disconnections were found to be of the same nature [35-37].

As such, in the present study, grain growth at general GBs in $SrTiO_3$ was studied in-situ using high resolution TEM (HRTEM), where anisotropic disconnection motion was detected. An example of a special GB is demonstrated as well (Figure 1a,b). Thermodynamic and kinetic aspects of disconnection motion are discussed, in light of the ex-situ results acquired for $SrTiO_3$ in the past. In a similar manner, the free surfaces of $SrTiO_3$ grains were studied in-situ, and anisotropic motion of ledges and terraces was recorded and compared to in-situ and ex-situ results acquired at general GBs in $SrTiO_3$.

To do so, thin films of polycrystalline $SrTiO_3$ were deposited on (001) surfaces of rock salt NaCl single crystal substrates (99.9%, SPI- Chem, USA) by pulsed layer deposition (PLD, MBE/ PLD-2100 deposition system, PVD Products Inc.) equipped with a KrF pulsed excimer

laser beam (λ=248 nm, COMPex PRO 102 Excimer Laser, Lambda Physik / Coherent), using a single crystal of $SrTiO_3$ (KMT Corporation) target. The deposition conditions were as follows; 60mTorr of O_2, the set point temperature was 500, 600 or 700ºC, the distance between target and substrate was 75mm, the laser fluency at the surface of the target was ~0.9 J/cm^2 and the frequency of pulses was 3 Hz. The films were transferred to heating chips (DENSsolutions "Through-Hole" reaching up to 1300°C) by dissolving the rock salt substrates in water (HPLC Water Plus, Sigma- Aldrich) after deposition. The films were then heated in-situ (DH30-4M double tilt DENSsolutions holder) in an aberration corrected TEM (FEI Titan 80-300 kV S/TEM) (see Figure S1 acquired before heating).

Each interface (GB or surface) was characterized edge-on, where both characteristic planes (GB and step planes in the case of GBs, and terrace and ledge planes in the case of surfaces) were parallel to the incident electron beam direction. This way the disconnections and the terraces and ledges can be discerned (rather than only their projection). In this work the edge-on GB and step planes as well as the terraces and ledges are defined as parallel to crystallographic planes in either of the delimiting grains (defined schematically in [35] for GBs).

Figure 1a,b presents disconnections detected along an edge-on GB annealed in-situ at 1040°C in vacuum, where the GB and step planes were parallel to (100) and (110) planes of both delimiting grains, which were both oriented in or close to a [001] zone axis (ZA). This GB is a *near* ∑5 orientation [41-43]. During heating the boundary migrated as a result of disconnections moving along the GB plane (Movie 1). Figure 1a,b indicates that within the 6.7 s that passed between the two images, the boundary and the disconnections changed their position, indicating movement. Minor grain rotation of the grain on the right is noted, which

could be associated with motion of the dislocation component of the disconnections as a result of GB migration, in addition to some minor tilting/ bending of the film. Disconnection motion was not continuous, and stagnation occurred between sequential disconnection motion, which is associated with the presence of an energy barrier for disconnection motion. For corroboration, Figure 1c,d,e,f (Movie 1 and Movie 2) indicate disconnection motion along two general GBs which are far from a high-symmetry orientation, heated in-situ to 1040°C. As demonstrated in Figure 1c,d (Movie 1) the GB and step planes were parallel to {001} and {110} planes of the grain on the left (oriented close to a [001] ZA). Later (Figure S2), the grain on the right tilted and rotated such that GB and step planes parallel to {110} planes were detected along this grain (then oriented close to a [111] ZA and the GB and step planes on the grain on the left keep their orientation). In the vicinity of the boundary presented in Figure 1c,d, above or below the grain on the right, a grain is forming and moving along the surface of the grain on the right. During the time presented in Figure 1c,d this particle did not interact with the boundary and thus did not affect it. The same anisotropy remained after interaction between the GB and the particle (Figure S2 and Movie 1). In Figure 1e,f (Movie 2) the GB and step planes were parallel to {001} and {110} planes along a grain oriented in the [001] ZA. The same anisotropic motion of disconnections was detected between the grain on the upper right part aligned close to the [001] ZA and the grain in the middle. The contrast indicated by the dashed yellow lines in Figure 1 emanates from inclined steps as explained in [37].

Figure 2 (Movie 3) present HRTEM micrographs of $SrTiO_3$ grains heated to 1040°C in-situ. Disconnection motion is demonstrated at two general GBs (Figure 2a,b and Figure 2c,d). In both cases the GB and step planes were parallel to {001} and {110} planes. Inclined steps were detected as well, and were assumed to be of the same nature as the edge-on ones (given the resulting artifacts). The boundary between the grain close to the [111] ZA and the grain close

to the [001] ZA on the bottom left (Figure 2d) also had disconnections along the same crystallographic planes.

Figure 3 (Movie 4) demonstrate disconnection motion at a GB in $SrTiO_3$ annealed in-situ to 1050°C in vacuum. A tilt angle of 12° exists between the grains in addition to a small twist angle. The dislocations along the boundary do not fit the Read- Shockley theory describing low angle GBs as an array of lattice dislocations [44], indicating that such a tilt angle falls within the regime of high angle GBs for $SrTiO_3$. The GB and step planes were parallel to {001} and {110} planes of both delimiting grains, both oriented in the [001] ZA. Inclined GB and step planes along the boundary may lead to contrast emanating from GB dislocations as if the dislocations are delocalized from the GB plane [37]. This explains the contrast indicated by the white arrow in Figure 3c. These inclined GB and step planes are assumed to be of the same nature as the edge-on planes [37].

Figure S2, Figure S3 and Movie 5 present additional examples for anisotropic disconnection motion at general GBs, in agreement with those discussed above. These figures and movies indicate not only that disconnections are present at general GBs, but that they are active during grain growth. As such, anisotropic disconnection motion is the mechanism by which general GBs migrate in $SrTiO_3$.

GB and step planes of the same nature were also detected at general GBs in $SrTiO_3$ annealed ex-situ, regardless of the experimental conditions [35,36,37]. In these samples GB and step planes were mainly parallel to {001} and {110} planes, whereas a specific pair of planes was detected depending on the orientation of the delimiting grains which were close to a low index ZA once the boundary was edge-on. For example, GB and step planes were detected parallel

to {001} and {110} planes along grains oriented in (or close to) a <001> ZA whereas they were parallel to {110} planes along grains oriented close to a <111> ZA. It should be noted that these specific crystallographic planes were found to be low energy planes in $SrTiO_3$ annealed under high oxygen partial pressures (comparable with the vacuum conditions used in this work, see supplementary material) [45-47]. The agreement between in-situ results presented in this manuscript and ex-situ results [35-37] confirms that disconnections at general GBs are similar in nature to those at special GBs (Figure 1a,b), where the same crystallographic anisotropy of disconnections was detected for both types of boundaries, and both migrate via anisotropic motion of disconnections.

Applying the dislocation analysis presented in [36] on the boundaries presented in Figure 1, Figure 2 and Figure 3 results in sums of the edge component of the dislocations being parallel to {001} and {110} planes, as was demonstrated ex-situ [36]. This confirms that both the step and the dislocation components of the disconnections characterized in-situ and ex-situ are in agreement.

Moving ledges and terraces were also detected in-situ at surfaces. For example, Figure 4 (Movie 6) present HRTEM micrographs of $SrTiO_3$ grains heated to 990°C in-situ, where the grain shrunk until it disappeared by the motion of ledges. As demonstrated in Figure 4, the ledges and terraces were parallel to {001} and {110} planes. While in the past ledges and terraces were detected on $SrTiO_3$, it was shown that they evolved mainly along TiO_x layers that developed on the surface of the $SrTiO_3$ grains [5]. In the results presented here secondary phases were not detected at the surface. We assume that the main driving force for shrinkage is surface area reduction by evaporation (which may have been accelerated by electron irradiation damage). It is also possible that ledges on the surface are active in surface

reconstruction [48-50].While ledges moved in a specific direction, in several cases and for short instances, they also moved in the opposite direction (condensation instead of evaporation; see Figure 4 and Figure S4). Ledge motion at surfaces was discontinuous, where stagnation occurred between sequential ledge motion, presumably associated with an energy barrier for ledge motion and formation of new ledges. The overall velocity of the ledges is thus dictated mainly by the duration of stagnation between sequential ledge movements, since ledge movement itself is rather fast. This indicates that the ledge motion process is strongly dependent on thermodynamic factors.

Given the anisotropy of the surface and GB energy in $SrTiO_3$ [45-47] we assume that the ledges and terraces identified in edge-on condition are responsible for accommodating the macroscopic shape of the particle and therefore may also be inclined to the electron beam direction at certain regions of the surface. Examples for such inclined ledges and terraces are marked by the dashed yellow lines in Figure 4a and the yellow dashed arrow in Figure 4c. A region with varying width (as a function of time) is noted in the right corner of the grain (marked by a dashed yellow arrow in Figure 4b), and is associated with artifacts resulting from inclined ledges and terraces. The inclined ledges and terraces are assumed to be of the same nature as the edge-on ledges and terraces (as noted in Figure 4a,c). Due to motion of these inclined ledges and terraces in the thickness of the specimen, the relative thickness of the grains changed in the vicinity of the edge-on ledges and terraces, resulting in changes in the contrast in the HRTEM micrographs (see for example the dashed yellow lines in Figure 4a).

While in Figure 4 the ledges and terraces parallel to {100} and {110} planes were visible along the surface of the grain aligned close to a [001] ZA, in a grain aligned close to the [111] ZA, the ledges and terraces were parallel to {110} planes (see lower part of Figure 2c and

supplementary material). This was in agreement with the nature of the GB and step planes of the disconnections detected in-situ and ex-situ at general GBs in $SrTiO_3$ [35]. All additional figures and movies (besides Figure S1) present additional examples for anisotropic ledge motion at the surface of the grains.

The results presented here indicate the anisotropic nature and motion of disconnections at general GBs, annealed in vacuum. The disconnection motion during in-situ experiments confirms not only that disconnections are present at general GBs in $SrTiO_3$, but also that they play an active role in grain growth. As such, it is concluded that anisotropic disconnection motion is the mechanism by which general GBs migrate in $SrTiO_3$. Motion of disconnections exhibiting the same anisotropy was demonstrated at a near-coincidence ($\sum$) GB, indicating that the migration mechanism for high and low symmetry GBs is the same. In addition, ledges and terraces were shown to move at grain surfaces, indicating similar anisotropy to disconnections detected at GBs. These results are in agreement with ex-situ results acquired from multiple general GBs in $SrTiO_3$ confirming the same specific anisotropy.

Acknowledgments: The authors acknowledge Maya and Max Raskin for their assistance with writing a code for adding time stamps in the Movies. **Funding:** This work was partially supported via a German-Israel Fund (GIF) grant No. I-1276-401.10/2014. **Competing interests:** The authors declare no competing interests.

References:

1. W.K. Burton, N. Cabrera, F.C. Frank, Philos. T. R. Soc. Lond. S-A, 243 (1951) 299-358.
2. A.J. Gratz, S. Manne, P.K. Hansma, Sci. 251 (1991) 1343-1346.

3. G.C. Weatherly, Acta Metall. 19 (1971) 181-192.
4. G. Koster, B.L. Kropman, G.J.H.M. Rijnders, D.H.A. Blank, H. Rogalla, Appl. Phys. Lett. 73 (1998) 2920-2922.
5. E. Liberti, A.I. Kirkland, Phys. Status. Solidi. A, 215 (2018) 1800394.
6. H. Gleiter, Acta Metall. 17 (1969) 565-573.
7. H. Gleiter, Acta Metall. 17 (1969) 853-862.
8. J.P. Hirth, R.C. Pond, Acta Mater. 44 (1996) 4749-4763.
9. R.C. Pond, J.P. Hirth, Defects at Surfaces and Interfaces, in: E. Henry, T. David (Eds.), Solid State Physics, Academic Press, 1994, pp. 287-365.
10. D.L. Medlin, D. Cohen, R.C. Pond, Philo. Mag. Lett. 83 (2003) 223-232.
11. R.C. Pond, X. Ma, J.P. Hirth, T.E. Mitchell, Philo. Mag. 87 (2007) 5289-5307.
12. H.A. Khater, A. Serra, R.C. Pond, J.P. Hirth, Acta Mater. 60 (2012) 2007-2020.
13. J.M. Howe, R.C. Pond, J.P. Hirth, Prog. Mater. Sci. 54 (2009) 792-838.
14. R.C. Pond, P. Shang, T.T. Cheng, M. Aindow, Acta Mater. 48 (2000) 1047-1053.
15. R. Pond, X. Ma, Y. Chai, J. Hirth, in: F. R. N. Nabarro and J. P. Hirth, Topological modelling of martensitic transformations, in: Dislocations in Solids, North-Holland, Amsterdam, 2007, pp. 225-261.
16. J.P. Hirth, J. Phys. Chem. Solids, 55 (1994) 985-989.
17. J.P. Hirth, G. Hirth, J. Wang, P. Natl. A. Sci. 117 (2020) 196.
18. N. Combe, F. Mompiou, M. Legros, Phys. Rev. Mater. 3 (2019) 060601.
19. J. Han, S.L. Thomas, D.J. Srolovitz, Prog. in Mater. Sci. 98 (2018) 386-476.
20. C. Wei, S.L. Thomas, J. Han, D.J. Srolovitz, Y. Xiang, J. Mech. Phys. Solids, 133 (2019) 103731.
21. S.J. Zheng, X.L. Ma, T. Yamamoto, Y. Ikuhara, Acta Mater. 61 (2013) 2298-2307.
22. M.J. Mills, Mater. Sci. Eng. A, 166 (1993) 35-50.
23. X. Zhao, H. Chen, N. Wilson, Q. Liu, J.-F. Nie, Nat. Commun. 10 (2019) 3243.
24. A. Rajabzadeh, F. Mompiou, S. Lartigue-Korinek, N. Combe, M. Legros, D.A. Molodov, Acta Mater. 77 (2014) 223-235.
25. S.E. Babcock, R.W. Balluffi, Acta Metall. 37 (1989) 2357-2365.
26. S.E. Babcock, R.W. Balluffi, Acta Metall. 37 (1989) 2367-2376.
27. K.L. Merkle, L.J. Thompson, F. Phillipp, Phys. Rev. Lett. 88 (2002) 225501.
28. K.L. Merkle, L.J. Thompson, Mater. Lett. 48 (2001) 188-193.
29. S.B. Lee, Y.M. Kim, Acta Mater. 57 (2009) 5264-5269.
30. K.L. Merkle, L.J. Thompson, F. Phillipp, Interface Sci. 12 (2004) 277-292.
31. S.G. Song, Philos. Mag. Lett., 79 (1999) 511-517.
32. Q. Zhu, G. Cao, J. Wang, C. Deng, J. Li, Z. Zhang, S.X. Mao, Nat. Commun. 10 (2019) 156.
33. T. Radetic, C. Ophus, D.L. Olmsted, M. Asta, U. Dahmen, Acta Mater. 60 (2012) 7051-7063.
34. A. Rajabzadeh, M. Legros, N. Combe, F. Mompiou, D.A. Molodov, Philos. Mag. 93 (2013) 1299-1316.

35. H. Sternlicht, W. Rheinheimer, M.J. Hoffmann, W.D. Kaplan, J. Mater. Sci. 51 (2016) 467-475.
36. H. Sternlicht, W. Rheinheimer, R.E. Dunin-Borkowski, M.J. Hoffmann, W.D. Kaplan, J. Mater. Sci. 54 (2019) 3694-3709.
37. H. Sternlicht, W. Rheinheimer, J. Kim, E. Liberti, A.I. Kirkland, M.J. Hoffmann, W.D. Kaplan, J. Mater. Sci. 54 (2019) 3710-3725.
38. W. Rheinheimer, M.J. Hoffmann, Scr. Mater. 101 (2015) 68-71.
39. M. Baurer, D. Weygand, P. Gumbsch, M.J. Hoffmann, Scr. Mater. 61 (2009) 584-587.
40. W. Rheinheimer, M. Bäurer, C.A. Handwerker, J.E. Blendell, M.J. Hoffmann, Acta Mater. 95 (2015) 111-123.
41. J. Cheng, J. Luo, K. Yang, Comp. Mater. Sci. 155 (2018) 92-103.
42. V. Ravikumar, V.P. Dravid, D. Wolf, Interface Sci. 8 (2000) 157-175.
43. V.P. Dravid, V. Ravikumar, Interface Sci. 8 (2000) 177-187.
44. W.T. Read, W. Shockley, Phys. Rev. 78 (1950) 275-289.
45. T. Sano, D.M. Saylor, G.S. Rohrer, J. Am. Ceram. Soc., 86 (2003) 1933-1939.
46. D.M. Saylor, B. El Dasher, T. Sano, G.S. Rohrer, J. Am. Ceram. Soc., 87 (2004) 670-676.
47. W. Rheinheimer, M. Bäurer, H. Chien, G.S. Rohrer, C.A. Handwerker, J.E. Blendell, M.J. Hoffmann, Acta Mater., 82 (2015) 32-40.
48. M. Kawasaki, K. Takahashi, T. Maeda, R. Tsuchiya, M. Shinohara, O. Ishiyama, T. Yonezawa, M. Yoshimoto, H. Koinuma, Sci, 266 (1994) 1540.
49. O. Warschkow, M. Asta, N. Erdman, K.R. Poeppelmeier, D.E. Ellis, L.D. Marks, Surf. Sci. 573 (2004) 446-456.
50. G.-z. Zhu, G. Radtke, G.A. Botton, Nat. 490 (2012) 384-387.

Figure Captions

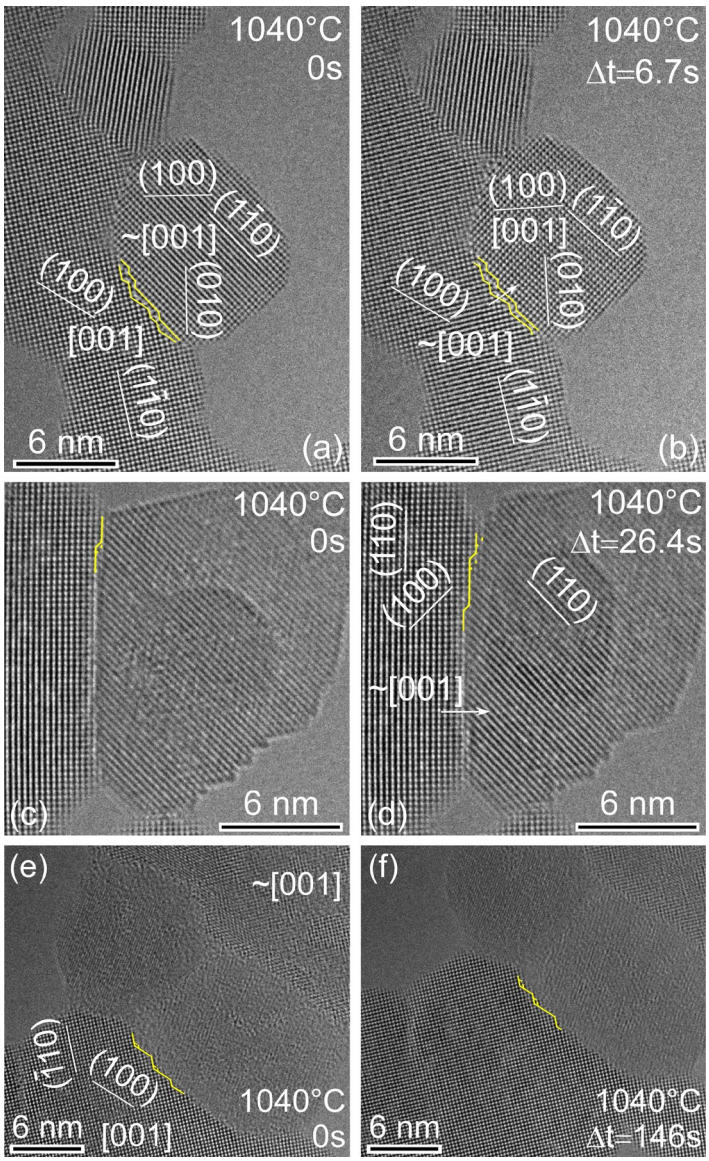

Figure 1: HRTEM micrographs of $SrTiO_3$ heated to 1040°C in-situ. (b) was acquired 6.7s after (a). (d) was acquired 26.4s after (c), and (f) was acquired 146s after (e). The yellow lines indicate the position of the GB and step planes along an edge-on GB which is a near ∑5 orientation relationship (a,b) and two edge-on general high-angle GBs (c,d and e,f). The arrows indicate the direction of the GB migration. The dashed yellow lines indicate inclined steps. Cs=-2.9µm.

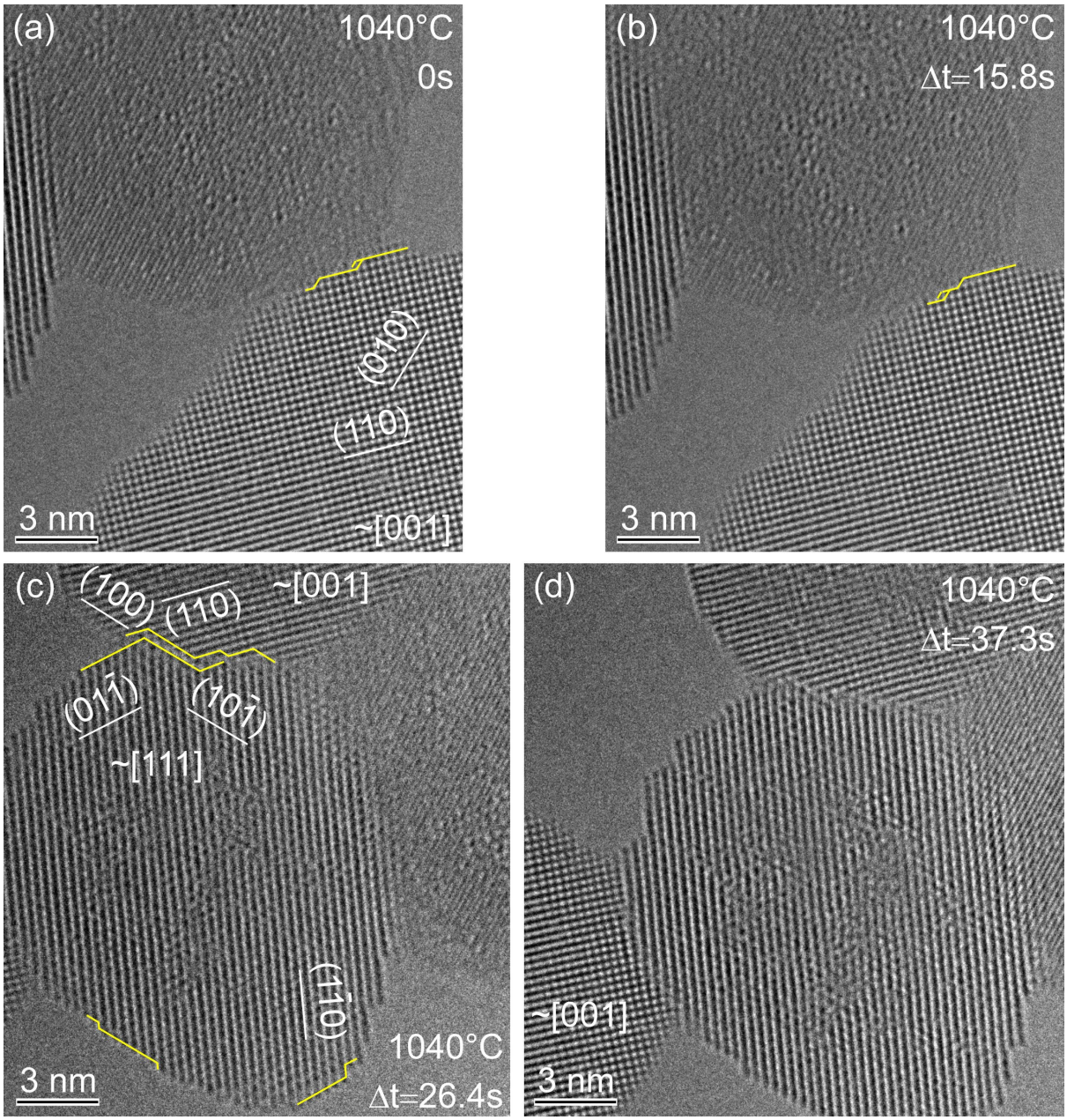

Figure 2: HRTEM micrographs of $SrTiO_3$ heated to 1040°C in-situ. (a)- (d) were acquired at time differences of 15.8s, 26.4s and 37.3s. The yellow lines indicate the position of the GB and step planes along two edge-on general high-angle GBs, as well as ledges and terraces along the grains. The dashed yellow lines indicate inclined steps. Δt indicates the time difference between a micrograph and the previous one. Cs=-2.9µm.

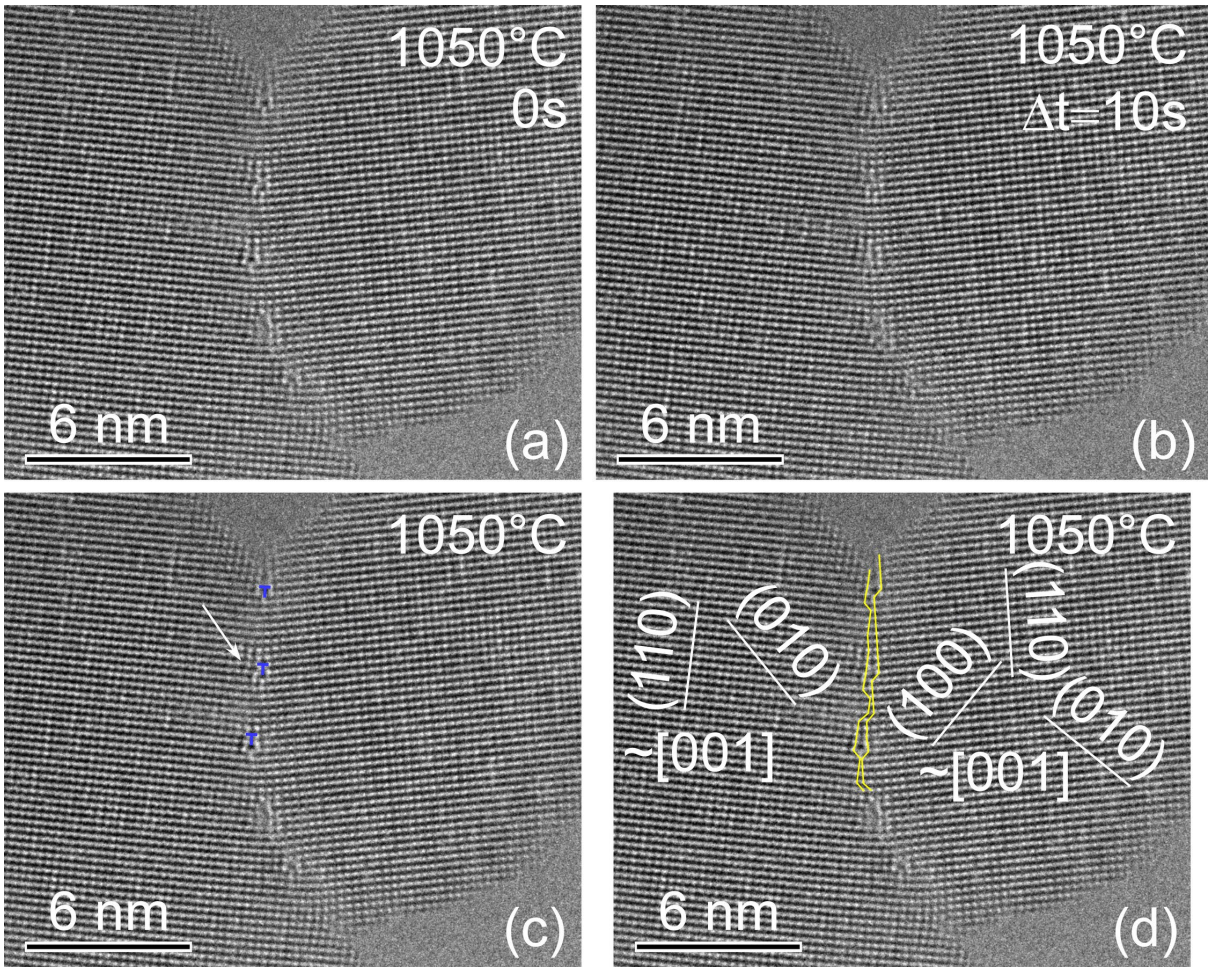

Figure 3: HRTEM micrographs of $SrTiO_3$ heated to 1050°C in-situ. (b) was acquired 10s after (a). (c) and (d) represent a suggested model for dislocations along the boundary (blue lines in (c)) and GB and step planes (yellow lines in (d)) analyzed in the specific edge-on state presented in (a). In this description ((c) and (d)) inclined steps were omitted but their presence can be inferred. Cs=-2.9µm.

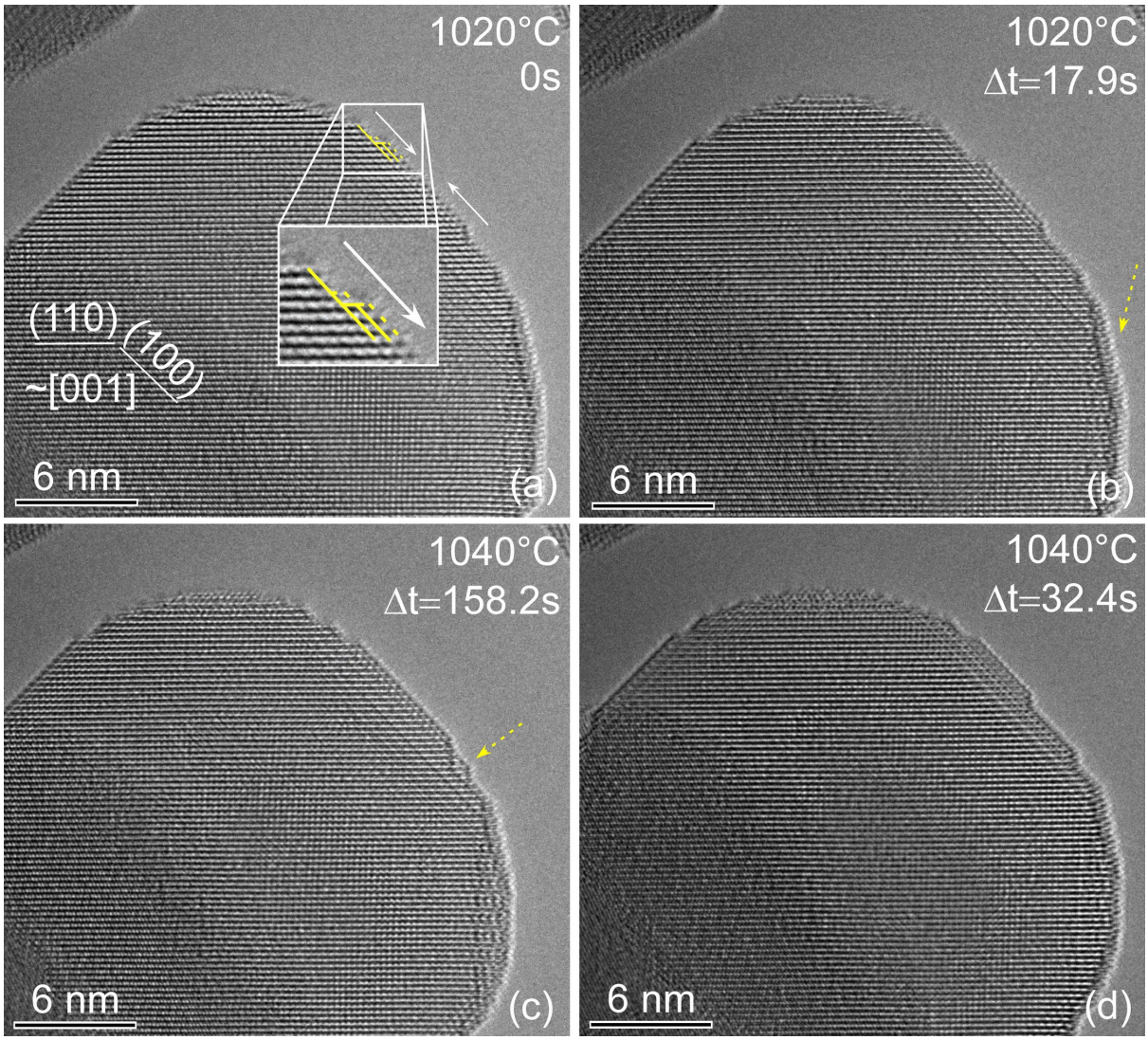

Figure 4: HRTEM micrographs of $SrTiO_3$ heated to 1020°C and 1040°C in-situ. (a)- (d) were acquired at time differences of 17.9s, 158.2s and 32.4s. The yellow lines indicate the position of ledges and terraces along the edge-on surface of a grain oriented close to a [001] zone axis. The dashed yellow lines and arrows indicate inclined ledges and terraces. The white arrows indicate the directions of the motion of the ledges. Cs=-5.9µm.

Graphical Abstract